Molten barium titanate, a high-pressure liquid silicate analogue

O.L.G. Alderman,[a,*] C.J. Benmore,[b] J. Neuefeind,[c] A. Tamalonis,[a] R. Weber[a,b]

a. Materials Development, Inc., Arlington Heights, IL 60004, USA.

b. X-Ray Science Division, Advanced Photon Source, Argonne National Laboratory, Argonne, IL 60439, USA

c. Chemical and Engineering Materials Division, Oak Ridge National Laboratory, Oak Ridge, TN 37830, USA

*Corresponding author o.alderman@gmail.com

The structure of molten $BaTiO_3$ has been measured using laser heating, aerodynamic levitation and a combination of neutron diffraction with Ti isotope substitution, x-ray diffraction and spectroscopy. All measurements point to a Ti–O coordination of n_{TiO} = 4.4(2), far lower than the perovskite or hexagonal crystalline forms. Nonetheless, $n_{TiO} > 4$ suggests structural analogy with high-pressure molten silicates. We introduce methodology for ascertaining such analogies and demonstrate similarity with molten $CaSiO_3$ at upper mantle pressures *circa* 5 GPa. Although some topological differences exist, we propose that planetary melt analogues provide rich insight into important processes relevant to hot exoplanets and Earth's early history, complementary to *in-situ* high *P-T* experiments and calculations.

Crystalline titanates have long been of mineralogical interest as analogues for silicates at extremes of pressure [1-3], with the distinct advantage of being accessible at ambient, or lower-pressures. In this Letter we investigate the extension of this analogy to the liquid state, using a series of experiments to elucidate the structure of molten $BaTiO_3$, followed by comparison to an appropriate silicate analogue. We suggest that the approach provides useful insight into the behavior of geophysically relevant high-pressure silicate melts. Furthermore, this insight is complementary to *in-situ* high *P–T* studies which are far more challenging for refractory liquids, as compared to their crystalline counterparts.

Our results have additional implications for the understanding of crystal nucleation, phase selection and growth of ferroelectric materials from the melt [4], the behavior of titanate-rich slags during upgrading of ilmenite ores [5], and the phenomenon of titanate glass formation. Indeed, liquids close to the $BaTi_2O_5$ composition can be quenched directly to form glasses with very high refractive indices [6,7]. These have application commercially as microspheres for retroreflective coatings, and show promise as lenses in super-resolution optical microscopy [8].

Three sets of experiments were performed to provide insight into different aspects of the structure of molten $BaTiO_3$, and the results combined to provide accurate atomistic models. All measurements exploited the aerodynamic levitation technique, combined with CO_2 laser heating, which allows access to

refractory liquids without contamination or constraints arising from a solid container [7,9-13]. In each case the temperature was close to 2100 K [14], ~200 K in excess of the melting point, T_{melt} = 1893 K.

Neutron diffraction with titanium isotope substitution was performed at the NOMAD beamline of the Spallation Neutron Source, Oak Ridge, TN, USA. The experimental and data analysis procedures are described elsewhere [13]. Two $BaTiO_3$ molten samples were measured [14], one enriched in 46-Ti, the other in 48-Ti, yielding mean bound coherent neutron scattering lengths for titanium of $\bar{b}_{46}$ = 4.47(5) fm and $\bar{b}_{48}$ = –5.49(2) fm respectively (the natural isotopic abundance value is $\bar{b}_{\mathrm{Nat}}$ = –3.370(13) fm [15]). Although less elegant than taking full advantage of the existence of both positive and negative scattering length isotopes to produce a null scattering sample, this approach was chosen to maximize the coherent scattering intensity of Ti-containing pair terms, resulting in a first order difference function with enhanced signal-to-noise. This approach is favored when small samples and limited counting times are necessary, such as in levitation experiments on high-temperature melts. In the present case, levitated liquid droplets of ~3.2 mm diameter where each measured for durations > 120 minutes [14].

X-ray diffraction was performed at the 11-ID-C beamline of the Advanced Photon Source (APS), Argonne, IL, USA. Selection of a high-energy (114.77 keV, λ = 0.10803 Å) beam of monochromatic x-rays greatly reduces corrections due to absorption, fluorescence and multiple scattering, as compared to lower energies, and increases the accessible momentum transfer magnitude, $Q = 4\pi\sin(\vartheta)/\lambda$, for a given scattering angle, 2ϑ. Full experimental details are described elsewhere [13]. It is important to note that the x-ray diffraction is dominated by Ba-containing pair terms in the present case, yielding highly complementary information to the neutron scattering measurements [14].

Bulk density is a key physical property which is strongly influenced by the atomic structure, and is required in the analysis of total scattering diffraction data. The density of molten $BaTiO_3$ has previously been measured using a shadow-casting technique applied to droplets heated with a CO_2 laser and held within a pressurized aerodynamic-electrostatic levitator operating at 450 kPa of air [16]. The measurements yielded a temperature dependent density of $\rho_m = 4.04 - (3.4 \times 10^{-4})(T - T_{\mathrm{melt}})$ in gcm^{-3} (T_{melt} = 1893 K) which we rely on in our analyses, and which is notably ~20% lower than the that of the crystalline solid.

Further complementary and element specific information pertinent to the local Ti environments was obtained using Ti K-edge x-ray absorption near-edge structure (XANES) spectroscopy, as described in Ref. [7], utilizing beamline 20-BM-B of the APS. The near-edge region does not suffer from the severe Debye-Waller damping pertaining to the extended x-ray absorption fine structure (EXAFS) at high temperatures, and is sensitive to both local structure and oxidation state.

The normalized XANES spectra plotted in Fig. 1 indicate dramatic structural differences between the ambient pressure perovskite phase and the high-temperature melt. While the TiO_6 octahedral symmetry in the crystal permits only weak quadrupolar 1s-3d pre-edge transitions, the intense peak for the liquid indicates dipolar transitions enabled by p-d hybridization in lower coordination sites [17]. Comparison of the liquid $BaTiO_3$ pre-edge peak height (0.57(6)) and position (4969.5(1) eV) to spectra for model compounds [18] indicates a mean Ti–O coordination number of $4 < n_{TiO} < 5$, arising from a mixture of TiO_4 tetrahedra with 5- and/or 6-fold Ti.

The three structure factor, $S(Q)$, measurements [14], and their real-space representations shown in Fig. 2, display greatly contrasting features arising from the variations in pair weighting factors. The Ti–O bond

length distribution is apparent in all three correlation functions, $T(r)$, as a peak *circa* 1.8 Å. This distance is close to that expected from TiO_4 tetrahedra. However, in all three cases, there is overlap with contributions from other pair terms at larger interatomic separations, particularly bonded Ba–O distances in the x-ray data, and both Ba–O and O–O in the neutron measurements. This overlap is eliminated in the first order difference function, $\Delta_{Ti}(r)$, between the two neutron correlation functions, which eliminates pair terms not containing Ti. The result (Fig. 2) has a Ti–O pair weighting of 79.2% [14] and indicates an asymmetric distribution of Ti–O bond lengths. Suitable integration of this peak up to a 2.75 Å cutoff yields n_{TiO} = 4.4(2), in excellent agreement with the semi-quantitative insight obtained from the Ti K-edge XANES, and consistent with the asymmetry of the peak which implies $n_{TiO} > 4$.

To gain insight into other aspects of the structure of molten barium titanate, a full atomistic model was derived using empirical potential structure refinement (EPSR) [19,20]. A total of 4800 atoms were held at a fixed density of ρ_m = 3.979 gcm^{-3} (0.05138 atoms Å^{-3}) and T = 2073 K. EPSR is akin to reverse Monte Carlo (RMC) modelling, but rather than the atomic positions, interatomic potentials defined between atom pairs are iteratively perturbed to obtain improved agreement with diffraction data. This is a natural way of incorporating additional constraints to ensure a physically plausible model. It can be seen in Fig. 2 that good agreement with the scattering data can be obtained. The Ti–O peak height is greater in the EPSR model compared to the 48-Ti neutron $T(r)$ and the $\Delta_{Ti}(r)$. This is likely due to uncertainty in the absolute normalization, which is greatest for the 48-Ti dataset due to the presence of both positive and negative pair weightings. Nonetheless, the Ti–O peak width is also narrower in the EPSR model, leading to a mean n_{TiO} = 4.39, in excellent agreement with the direct determination from $\Delta_{Ti}(r)$. The model also reveals that n_{BaO} = 7.13 such that both Ba–O and Ti–O coordination numbers are far lower than in the perovskite or hexagonal forms of $BaTiO_3$ (n_{TiO} = 6, n_{BaO} = 12).

In order to explore the putative analogy between molten barium titanate and liquid silicates at elevated pressures, we first consider the crystalline forms. $BaTiO_3$ is the archetypal ferroelectric perovskite, although a hexagonal phase also forms at high-temperatures. Silicate perovskite phases form at elevated pressures, e.g. $P \gtrsim 21$ GPa for $MgSiO_3$ (bridgmanite [21]), which is considered the most abundant mineral on Earth, or $P \gtrsim 11$ GPa for $CaSiO_3$, the third most. Hence there is a clear analogy between ambient-pressure titanates and high-pressure silicates. However, the lack of translational symmetry in liquids means that any analogy cannot be based on symmetry, but must consider the local structure. Given that silicate liquids and glasses tend to have $n_{SiO} > 4$ only at elevated pressures, then liquid $BaTiO_3$ satisfies at least this criterion. However, key questions that arise are:

i) At what temperatures should comparisons be made?
ii) Which aspect(s) of the local structure should be considered?
iii) To what 'silicate equivalent pressure', P^S, do our 2073 K molten titanate measurements correspond?

As we shall show, the answers to i-iii) are in fact all interdependent. We propose that scaling temperatures to the melting points provides a universal scale, such that

$$T^{\mathrm{S}} = T^{\mathrm{T}} \frac{T^{\mathrm{S}}_{\mathrm{melt}}(P^{\mathrm{S}})}{T^{\mathrm{T}}_{\mathrm{melt}}(0)}, \quad (1)$$

where superscripts S and T denote silicate and titanate respectively. However, the pressure dependence of $T^S_{melt}(P^S)$ renders T^S unknown without knowledge of P^S (iii). A straightforward means to address

questions ii) and iii) emerges if we consider the fact that a given silicate and titante structure can only ever be isomorphous within a length scaling factor, which can conveniently be taken as the tetravalent cation-oxygen bond length, r_{XO}. Hence the atom number densities should satisfy the following relationship

$$\rho^{\mathrm{S}}(P^{\mathrm{S}},T^{\mathrm{S}}) = \rho^{\mathrm{T}}(0,T^{\mathrm{T}})\left(\frac{r_{\mathrm{TiO}}(0,T^{\mathrm{T}})}{r_{\mathrm{SiO}}(P^{\mathrm{S}},T^{\mathrm{S}})}\right)^{3}. \quad (2)$$

We note here that the ratio $r_{\mathrm{TiO}}/r_{\mathrm{SiO}}$ for a given, common, site symmetry can be estimated from e.g. bond-valence parameters [22,23], and varies only weakly in the coordination number range of interest ($4 \le n_{XO} \le 6$), being $r_{\mathrm{TiO}}/r_{\mathrm{SiO}} \simeq 1.112(5)$. Since the divalent cation-oxygen distance should scale by the same amount, we suggest that any comparison of the molten $BaTiO_3$ structure is best made to high-pressure $CaSiO_3$, because calcium yields the most similar bond length ratio with barium to that stated above for Ti and Si. Specifically, $r_{\mathrm{BaO}}/r_{\mathrm{CaO}} \simeq 1.129(7)$ for $6 \le n_{MO} \le 12$.

Equations (1) and (2) can be solved simultaneously to provide the desired P^{S}–T^{S} coordinate. Conceptually this corresponds to the locus in the P^{S}–T^{S} plane of the melting curve, $T^{\mathrm{S}}_{\mathrm{melt}}(P^{\mathrm{S}})$, with the atom number density contour defined by equation (2). Ideally then, we would compare our structural model for molten $BaTiO_3$ to a model for molten $CaSiO_3$ at a single well-defined P^{S}–T^{S} coordinate derived from the experimental melting curve [24,25] and equation of state. However, the latter has not been directly determined experimentally. Furthermore, diffraction data, and therefore experimentally derived structure models, from high-pressure molten $CaSiO_3$ are limited [26], and indeed the difficulty of obtaining such data is precisely what motivates our search for analogues at ambient pressure. We therefore choose to compare our molten $BaTiO_3$ model to those predicted recently by first principles molecular dynamics (FPMD) over a range of pressures and temperatures [27]. A detailed comparison can be made directly between the set of six unique partial pair distribution functions, $g_{ij}(r)$, after scaling by r_{XO}. An example of such a comparison is shown in Fig. 3 for (P^{S},T^{S}) = (7.5 GPa, 4000 K), which also satisfies equation 2 (see Table 1). Before we discuss the details of Fig. 3, we first demonstrate that 7.5 GPa and 4000 K is close to the optimal state point for comparison. A similarity index can be defined by

$$R_{\chi} = \frac{2}{n^2+n}\sum_{j\ge i,i}^{n}\left(\frac{\sum_k r_k^{*2}\left[g_{ij}^{\mathrm{S}}(r_k^*)-g_{ij}^{\mathrm{T}}(r_k^*)\right]^2}{\sum_k r_k^{*2}\left[g_{ij}^{\mathrm{T}}(r_k^*)\right]^2}\right)^{1/2} = \frac{1}{6}\sum_{j\ge i,i}^{3} R_{\chi}^{ij}, \quad (3)$$

where n is the number of atomic species (3 in the present case) and $r^*_k = r_k/r_{XO}$ is the k^{th} bin in scaled space. $R\chi$ tends to zero only in the case of exact isomorphism, that is, identity between all six $g^{\mathrm{S}}_{ij}(r^*)$ with their corresponding $g^{\mathrm{T}}_{ij}(r^*)$. $R\chi$ for all three available temperatures and a range of pressures (corrected for Pulay forces [27]) are shown in Fig. 4. Minima are apparent for all three temperatures, but are most clearly pronounced at 3000 and 4000 K, close to $P^{\mathrm{S}} \simeq 5$ GPa. Note that only the third (central) point on each curve satisfies equation 2, and that minima occur here in $R\chi^{MM}$ [14]. What is strongly implied by Fig. 4 is that the structure of molten $BaTiO_3$ at 2073 K approaches that of liquid $CaSiO_3$ at $P^{\mathrm{S}} \simeq 5$ GPa, equivalent to upper mantle pressures on Earth at depths of 100 to 200 km. The temperature of 3000 to 4000 K is somewhat higher than expected from equation 1. Indeed, 5 GPa is below the pressure at which $CaSiO_3$ perovskite becomes stable, and the melting point is only $T^{\mathrm{S}}_{\mathrm{melt}}(5\ \mathrm{GPa}) \simeq 2000$ K, which yields $T^{\mathrm{S}} \simeq 2240$ K. Even using the metastable extension of the $CaSiO_3$ perovskite melting curve [25] yields only $T^{\mathrm{S}}_{\mathrm{melt}}{}'(5\ \mathrm{GPa}) \simeq 2600$ K, and $T^{\mathrm{S}} \simeq 2880$ K, from equation 1. The discrepancy may arise from a FPMD melting point in excess of that observed experimentally. Indeed, high-pressure melting curves calculated using density functional theory (DFT) for MgO are well in excess of experimental data [28], both with local density approximation (LDA)

and generalized gradient approximation (GGA). No melting instability was observed in DFT-GGA simulations of $CaSiO_3$ perovskite up to 29 GPa and 4000 K [29], well above the experimental melting curve [25]. Hence we can reasonably expect the DFT-LDA simulations of molten $CaSiO_3$, to which we make comparison in Fig. 3 and 4, to have a high melting point, consistent with our empirical T^S in the 3000 to 4000 K range.

We may now inspect the $g_{ij}(r^*)$ comparisons in Fig. 3 as a means to assess the extent of structural analogy. Most of the molten titanate pair distribution functions bear a very strong resemblance to their high-pressure silicate counterparts. A small low-r^* shoulder on $g_{BaBa}(r^*)$ is likely an artefact arising from systematic uncertainties in the neutron data normalization. The largest and most significant differences are between the $g_{XX}(r^*)$ for the tetravalent cations. The smaller structural length scale in the silicate leads to larger repulsive Coulombic forces between Si pairs, as compared to Ti pairs. This enhanced interaction appears to lead to a smaller n_{SiSi} (Table 1), even at the same scaled density, ρr^3_{XO}. The knock-on effects include a smaller $n_{SiO} < n_{TiO}$ (Table 1), and hence a different network topology in the silicate.

Nonetheless, based on the structural similarity demonstrated, a rich qualitative insight into upper mantle-pressure silicate melts can be gained from what is known experimentally about ambient pressure titanate liquids. This insight is independent of, and complementary to, both *ab-initio* calculations, and *in-situ* studies, with the great advantage of unique, high-quality data arising from simplified experiments. We can expect high-pressure melting of silicates to be accompanied by large decreases in Si–O coordination (at constant P), with major consequences for physical properties, and consistent with FPMD simulations [27,30]. Furthermore, the addition of modifier (e.g. CaO) will tend to decrease the Si–O coordination, as is shown to be the case for our $BaO\text{-}TiO_2$ analogues spectroscopically (Fig. 1) and by diffraction (*cf*. [7]). We have previously demonstrated a negative temperature coefficient, $\partial n_{TiO}/\partial T < 0$, for liquid TiO_2 [9] and $BaTi_2O_5$ [7], and a similar effect is observed for n_{SiO} in high-pressure silicates [27,30]. Indeed, whilst temperature induced structural changes are smaller than those induced by pressure, they are far from negligible. The negative $\partial n_{SiO}/\partial T < 0$ can be expected to increase liquid fragility and, combined with the elevated $n_{SiO} > 4$, glass formation will become ever more difficult as P increases. While tetrahedral carbonate networks might vitrify at ~100 GPa pressures [31] in the lower mantle, this still leaves a huge volume likely devoid of glass forming ability and attendant phenomena.

We suggest that wider experimental study of molten titanates, and other analogues for high-pressure planetary melts [32], should prove fruitful in understanding important phenomena in hot exoplanets, planetary formation, and the Earth's early history. The $BaO\text{-}CaO\text{-}Sc_2O_3\text{-}TiO_2$ quaternary is suggested as an analogue for the model basalt $CaO\text{-}MgO\text{-}Al_2O_3\text{-}SiO_2$ system. GeO_2-based melts may provide a window into shallower silicate liquid behavior, and 'anomalous' extrema in physical properties with composition, as observed for germanate glasses [33] should be sought.

Acknowledgements

Dr. Suraj Bajgain is thanked for helpful correspondence and provision of FPMD $g(r)$ for liquid $CaSiO_3$ [27].

Lawrie Skinner (XRD, ND), Sonia Tumber (XRD?), A. Lin (ND), Sam Sendelbach (XANES), S. Heald (XANES), C. Weiss (MD – not included).

Work was supported by U.S. Department of Energy (DOE) under grant number SBIR DE-SC0015241 (OLGA, AJT, JKRW). This research used resources of the Advanced Photon Source, a U.S. DOE Office of Science User Facility operated for the DOE Office of Science by Argonne National Laboratory under Contract No. DE-AC02-06CH11357, and of the Spallation Neutron Source, a DOE Office of Science User Facility operated by the Oak Ridge National Laboratory.

References

[1] R. C. Liebermann, L. E. Jones, and A. Ringwood, Phys. Earth. Planet. In. **14**, 165 (1977).
[2] J. Walsh, P. Taylor, A. Buckley, T. Darling, J. Schreuer, and M. Carpenter, Phys. Earth. Planet. In. **167**, 110 (2008).
[3] P. Li, S.-i. Karato, and Z. Wang, Phys. Earth. Planet. In. **95**, 19 (1996).
[4] J. Yu, P.-F. Paradis, T. Ishikawa, S. Yoda, Y. Saita, M. Itoh, and F. Kano, Chem. Mater. **16**, 3973 (2004).
[5] P. C. Pistorius, J. S. Afr. Inst. Min. Metall. **108**, 35 (2008).
[6] J. Yu, S. Kohara, K. Itoh, S. Nozawa, S. Miyoshi, Y. Arai, A. Masuno, H. Taniguchi, M. Itoh, M. Takata, T. Fukunaga, S.-y. Koshihara, Y. Kuroiwa, and S. Yoda, Chem. Mater. **21**, 259 (2009).
[7] O. L. G. Alderman, C. J. Benmore, A. Tamalonis, S. Sendelbach, S. M. Heald, and R. Weber, J. Phys. Chem. C **120**, 26974 (2016).
[8] A. Darafsheh, G. F. Walsh, L. Dal Negro, and V. N. Astratov, Appl. Phys. Lett. **101**, 141128 (2012).
[9] O. L. G. Alderman, L. B. Skinner, C. J. Benmore, A. Tamalonis, and J. K. R. Weber, Phys. Rev. B **90**, 094204 (2014).
[10] L. B. Skinner, C. J. Benmore, J. K. R. Weber, J. Du, J. Neuefeind, S. K. Tumber, and J. B. Parise, Phys. Rev. Lett. **112**, 157801 (2014).
[11] L. B. Skinner, C. J. Benmore, J. K. R. Weber, M. A. Williamson, A. Tamalonis, A. Hebden, T. Wiencek, O. L. G. Alderman, M. Guthrie, L. Leibowitz, and J. B. Parise, Science **346**, 984 (2014).
[12] J. W. E. Drewitt, L. Hennet, A. Zeidler, S. Jahn, P. S. Salmon, D. R. Neuville, and H. E. Fischer, Phys. Rev. Lett. **109**, 235501 (2012).
[13] O. L. G. Alderman, C. J. Benmore, J. C. Neuefeind, E. Coillet, A. Mermet, V. Martinez, A. Tamalonis, and J. K. R. Weber, Phys. Rev. Mater. **2**, 043602 (2018).
[14] See Supplemental Material at *URL to be inserted by publisher* for further experimental details and plots showing structure factors and further analyses.
[15] L. Koester, K. Knopf, and W. Waschkowski, Z. Phys. A: Hadrons Nucl. **345**, 175 (1993).
[16] J. Yu, T. Ishikawa, and P.-F. Paradis, J. Cryst. Growth **292**, 480 (2006).
[17] T. Yamamoto, X-Ray Spectrom. **37**, 572 (2008).
[18] F. Farges, G. E. Brown, and J. J. Rehr, Phys. Rev. B **56**, 1809 (1997).
[19] C. Landron, L. Hennet, T. E. Jenkins, G. N. Greaves, J. P. Coutures, and A. K. Soper, Phys. Rev. Lett. **86**, 4839 (2001).
[20] A. K. Soper, Phys. Rev. B **72**, 104204 (2005).
[21] O. Tschauner, C. Ma, J. R. Beckett, C. Prescher, V. B. Prakapenka, and G. R. Rossman, Science **346**, 1100 (2014).
[22] A. C. Hannon, J. Non-Cryst. Solids **451**, 56 (2016).
[23] N. E. Brese and M. O'Keeffe, Acta Crystallogr. B **47**, 192 (1991).
[24] A. Zerr, G. Serghiou, and R. Boehler, Geophys. Res. Lett. **24**, 909 (1997).
[25] Z. Wang, W. Griffin, S. O'Reilly, H. Zheng, and H. Mao, J. Phys. Chem. Solids **61**, 1815 (2000).
[26] N. Funamori, S. Yamamoto, T. Yagi, and T. Kikegawa, J. Geophys. Res.-Sol. Ea. **109** (2004).
[27] S. K. Bajgain, D. B. Ghosh, and B. B. Karki, Phys. Chem. Miner. **42**, 393 (2015).
[28] D. Alfè, Phys. Rev. Lett. **94**, 235701 (2005).

[29] L. Li, D. J. Weidner, J. Brodholt, D. Alfe, G. D. Price, R. Caracas, and R. Wentzcovitch, Phys. Earth. Planet. In. **155**, 249 (2006).
[30] B. B. Karki, D. Bhattarai, and L. Stixrude, Phys. Rev. B **76**, 104205 (2007).
[31] D. B. Ghosh, S. K. Bajgain, M. Mookherjee, and B. B. Karki, Sci. Rep. **7**, 848 (2017).
[32] B. Kalkan, B. Godwal, S. V. Raju, and R. Jeanloz, Sci. Rep. **8**, 6844 (2018).
[33] O. L. G. Alderman, A. C. Hannon, S. Feller, R. Beanland, and D. Holland, J. Phys. Chem. C **121**, 9462 (2017).

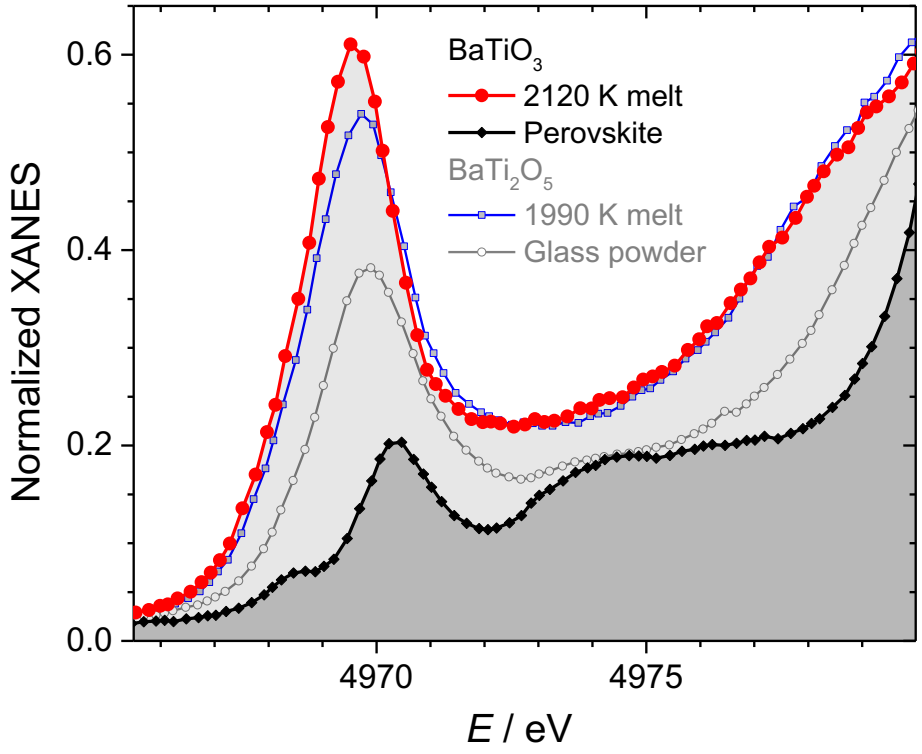

Figure 1: Pre-edge regions of the Ti K-edge XANES spectra obtained on levitated molten $BaTiO_3$ and the recovered perovskite powder transmission measurement. Shown for comparison are similarly obtained spectra for molten $BaTi_2O_5$ and the recovered glass [7].

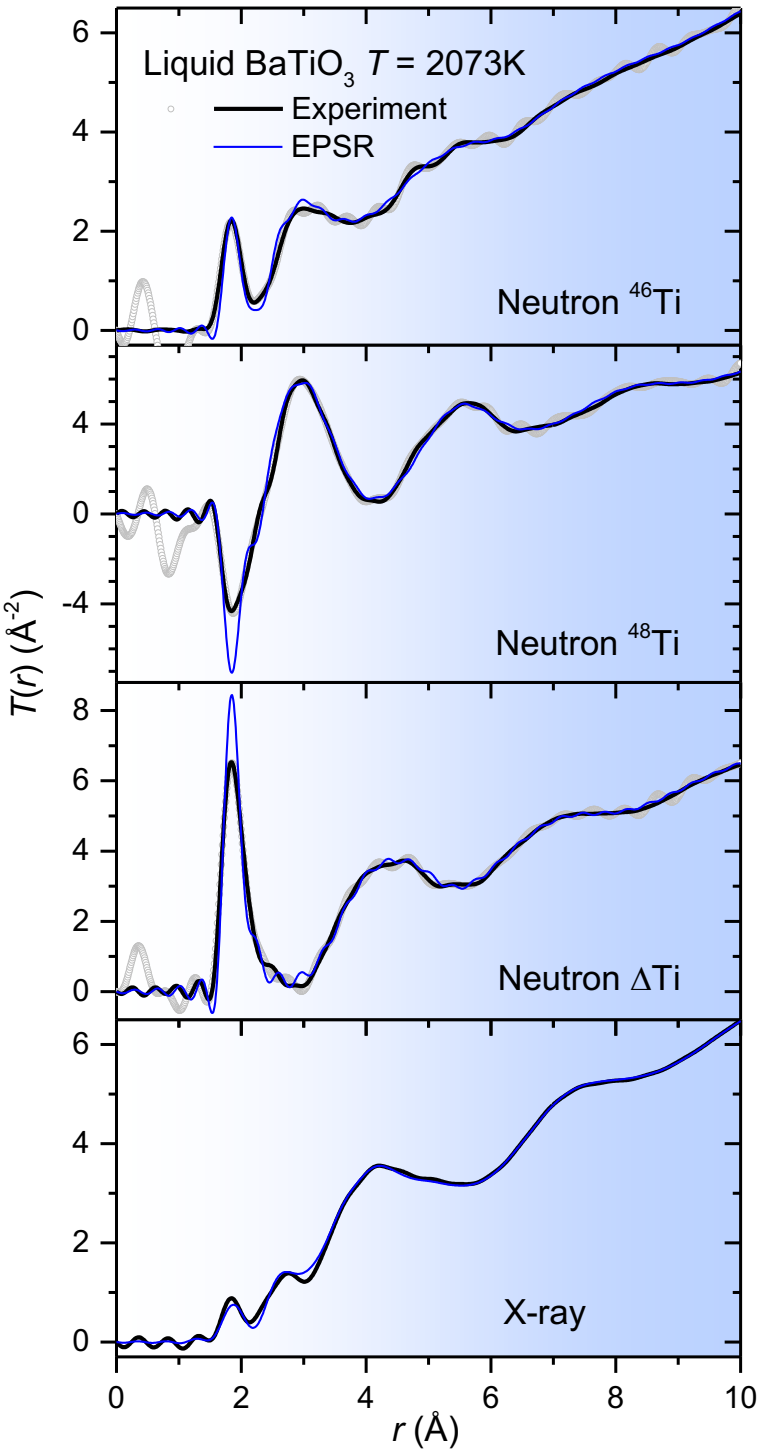

Figure 2: Total correlation functions for molten $BaTiO_3$ *circa* 2073 K. Two neutron diffraction measurements on samples enriched in Ti-46 and Ti-48 isotopes respectively are shown followed by their first-order difference (ΔTi) and the high-energy x-ray diffraction result. Direct comparison is made to EPSR derived (thin blue curves) structure models. Experimental data are shown as heavy black curves and in the neutron case, prior to Fourier filtering, as open grey circles.

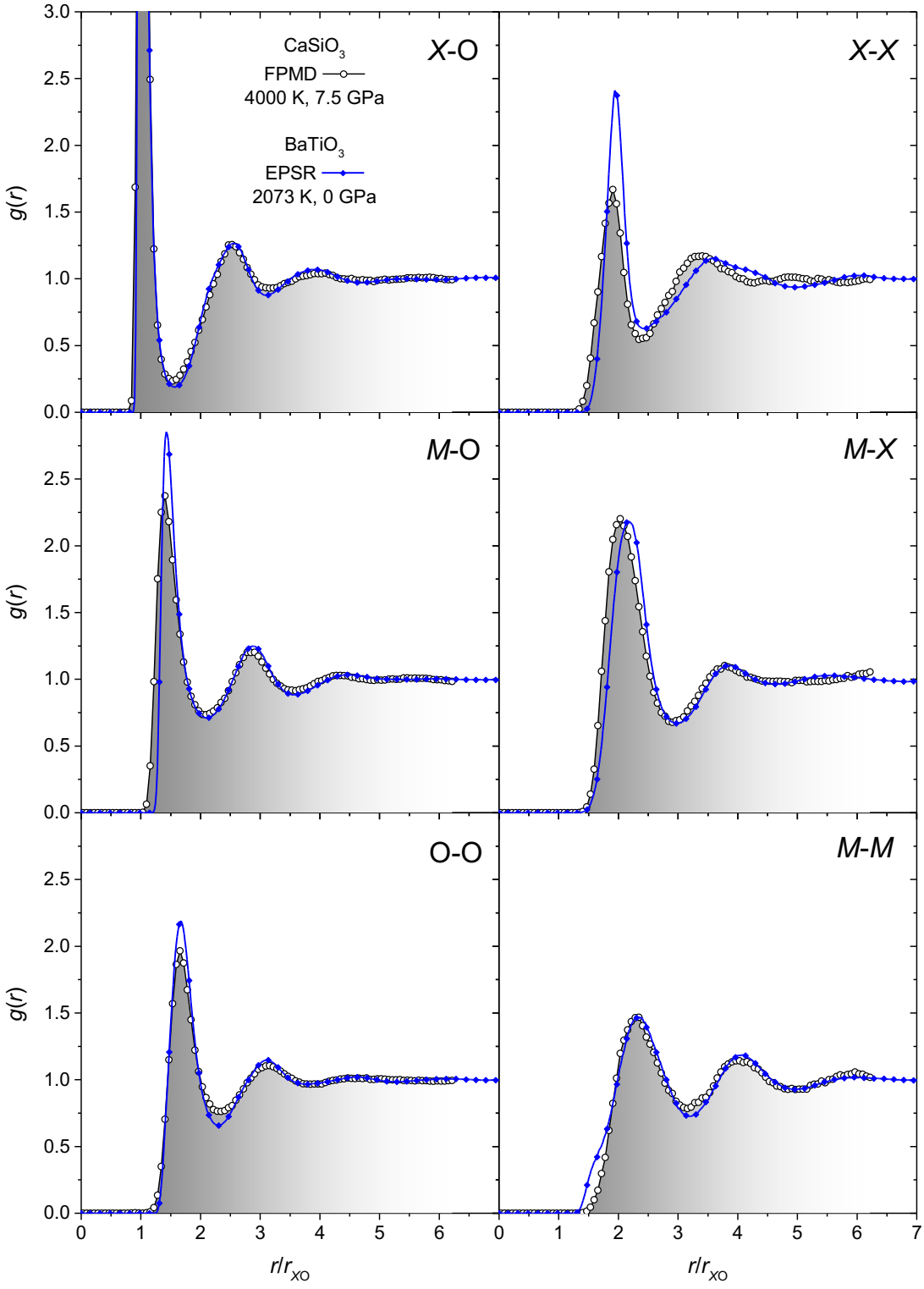

Figure 3: Partial pair distribution functions from liquid $BaTiO_3$, derived from the EPSR model, compared directly to those of high-pressure molten $CaSiO_3$ at 7.5 GPa and 4000 K, derived by FPMD [27]. All $g(r)$ for the MXO_3 liquids are plotted after length-scaling to the tetravalent cation-oxygen distance, r_{XO}, with r_{SiO} = 1.60 Å and r_{TiO} = 1.81 Å. Comparisons at other state points are shown in Ref. [14].

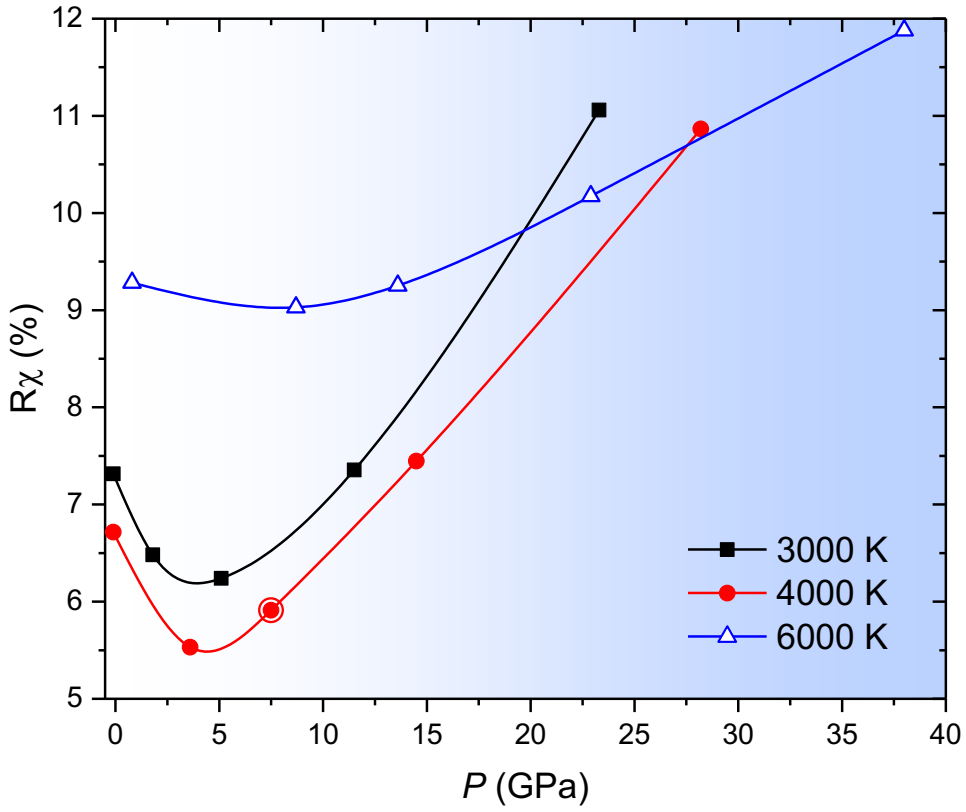

Figure 4: Mean similarity indices averaged over the six unique partial pair distribution functions, according to equation 3. The EPSR derived functions for barium titanate were used, whilst the pressure ordinate and temperatures correspond to those of FPMD calcium silicate melts [27]. The circled point at 4000 K corresponds to the functions plotted in Fig. 3. Lines are spline fits to guide the eye.

Table 1: Comparison of densities and coordination numbers between liquid $BaTiO_3$, and high-pressure molten $CaSiO_3$ [27].

Material	P (GPa)	T (K)	r_{XO} (Å)	$\rho\, r^3_{XO}$ (atoms)		X–O	M–O	O–O	X–X	M–X	M–M
					r_{cut}/r_{XO}	1.519	2.110	2.337	2.453	2.956	3.204
$BaTiO_3$ (*l*)	0	2073	1.81	0.30465	n_{ij}	4.386	7.126	9.204	3.319	6.931	7.610
$CaSiO_3$ (*l*)	7.5	4000	1.60	0.31002	n_{ij}	4.227	7.372	9.399	2.884	7.139	7.640
					n^T/n^S	1.038	0.967	0.979	1.151	0.971	0.996